The origin of additional modes in Raman spectra of ZnO:Sb films

Cai-Qin Luo[1,2], Lok-Ping Ho[2], Francis Chi-Chung Ling[2,a*]

[1]*Henan Key laboratory of Photovoltaic Materials, Henan University, Jin Ming Avenue, Kaifeng, P.R. China*
[2]*Department of Physics, The University of Hong Kong, Pokfulam Road, Hong Kong, P. R. China*

*Contact author: ccling@hku.hk

ABSTRACT

Systematic Raman spectroscopic study was conducted on the wurtzite (002) Sb-doped ZnO films grown by pulsed laser deposition with different Sb doping levels and annealed at different temperatures, with the undoped, Cu-doped and Ga-doped ZnO films for comparison. The as-grown Sb-doped ZnO samples having the Sb doping level <3 wt% (<4×10^{20} cm^{-3} in the sample) exhibited n^+-conductivity with $n^+>10^{20}$ cm^{-3}. Three additional Raman modes 235 cm^{-1}, 510 cm^{-1} and 534 cm^{-1} were observed only in the Sb-doped ZnO samples but not in the other controls. The vibration mode 235 cm^{-1} was associated to the Sb_{Zn}-related shallow donor, which was the origin of the n^+-conductivity. The 510 cm^{-1} vibrational mode has been associated to H_O in previous literatures. However in the current study, correlation between its intensity and the H abundance was not observed. The 534 cm^{-1} Raman mode was associated with a Sb-related defect. The variation of the intensities of the Raman modes 235 cm^{-1} and 510 cm^{-1} upon annealing and change of Sb composition were discussed.

Keywords

Raman additional modes, Sb-doped ZnO, Sb_{Zn} defect

INTRODUION

Wurtzite-type ZnO material has a wide band gap (3.37 eV) at room temperature and a large exciton binding energy (60 meV) [1]. ZnO attracts extensive attention because of its potential applications in optoelectronic [2], electronic and spintronic devices, etc [3]. The development of practical ZnO devices is hindered by the lack of a complete understanding of native and impurity defects in the ZnO lattice. For example, many theoretical and experimental studies associated the unintentional hydrogen impurities as the origin of the n-type conductivity in ZnO [4,5], but there was also recent report attributing V_O to the n-type conductivity of unintentional doped ZnO [6]. The green luminescence without fine structure, which is a commonly observed defect emission in ZnO materials, is controversial and has been attributed to the intrinsic defects Zn-vacancy and O-vacancy [7-10]. Sb-doped ZnO [11] (and so does As and P doped [12,13]) have been reported to be p-type conductive and the X_{Zn}-$2V_{Zn}$ (where X=Sb, As or P) was suggested to be the shallow acceptor [14]. However, there were also literatures reporting the n^+ conductivity (~10^{20} cm^{-3}) of Group-V doped ZnO [15,16]. Raman spectroscopy is an optical method capable of detecting dopants and impurities. Bundesmann et al [17] reported Raman vibration modes in ZnO specifically associated with some certain dopants, like the additional modes at 720 cm^{-1} for Fe, 531 cm^{-1} for Sb, and 631 cm^{-1} for Ga. Based on the combined results of photoluminescence (PL) and Raman studies, Kirste et al [18]

associated two vibrational modes (735 cm^{-1} and 1090 cm^{-1}) in Li-doped ZnO to be originated from the surface-bound LiO_2 defect sites. For the case Sb-doped ZnO, the relevant Raman studies are relatively few [17,19]. Zuo et al [19] observed the additional mode of 528 cm^{-1} with Sb-doping in Sb-doped ZnO nanocrystallites and its intensity increased with the Sb doping composition. The additional modes of 509, 532 and 575 cm^{-1} were reported by Paradowska et al [20] in Sb-doped ZnO films grown by molecular beam epitaxial (MBE). In another Raman study of MBE grown Sb-doped ZnO, Przeździecka et al [21] reported the Raman additional modes of 511, 533 and 575 cm^{-1} which were associated with the Sb doping.

In this paper, we reported a detailed Raman spectroscopic study on Sb-doped ZnO films fabricated by pulsed laser deposition (PLD). The systematic effects of the Sb composition and thermal annealing were investigatd. Three additional vibrational modes were found to be associated with the Sb doping. X-ray diffraction (XRD), transmission electron microscopic (TEM), room temperature Hall effect measurement and secondary ion mass spectroscopy (SIMS) were also conducted on the samples to reveal the structural and electrical properties of the samples so as to facilitate the understanding of the Raman results.

EXPERIMENTAL

Undoped ZnO, 1 wt% Ga doped, 1 wt% Cu doped and Sb doped ZnO thin films were fabricated on c-plane sapphire substrate by pulsed laser deposition (PLD). Sb_2O_3:ZnO ceramic targets with different Sb compositions of 0.5, 1, 2 and 3 wt%

(samples denoted by ZnO:Sb(0.5%), ZnO:Sb(1%), ZnO:Sb(2%) and ZnO:Sb(3%) respectively) were used for the laser ablation in the PLD growth. The purity of the target is 99.99 %. The oxygen partial pressure was kept at 1.3 Pa and the substrate temperature was 350℃ during the growth. A KrF laser with the wavelength of 248 nm, pulse energy of 300 mJ and the repetition frequency of 2 Hz was used to ablate the targets. The thickness of the films were ~300 nm. Post-growth annealing process for the Sb-doped ZnO samples was performed in the argon atmosphere at the temperatures of 500℃, 550℃, 600℃ and 650℃ for 30 minutes. The crystalline structure of the films was studied by high-resolution X-ray diffraction (XRD) and high-resolution transmission electron microscopy (HRTEM). The XRD study was performed with the Philip D5000 and Bruker D8 advance diffractometer. The TEM study was performed using the HRTEM-JEOL 2010F. The chemical composition depth profile was studied using secondary ion mass spectroscopy (SIMS) with the IONTOF TOF-SIMS V spectrometer. The carrier concentration of the Sb doped ZnO samples were studied by Hall measurement (Accenet HL-5500PC) at the room temperature. The Raman scattering measurement was performed at room temperature with the laser beam perpendicular to the film surface using the 514.5 nm excitation line of an Ar+ ion laser. All the Raman spectra were measured under a backscattering configuration ($z(-,-)\bar{z}$ in Porto notation) using the Renishaw inVia confocal Raman microscope. The Raman wavenumber was taken in the range of 100-1000 cm^{-1}. The laser power and acquisition time for all the Raman measurement was 25 mW and 1s respectively.

RESULTS AND DISCUSSION

The cross-sectional HRTEM image of the as-grown ZnO:Ga(2%) in Figure 1(a) reveals that the film grew along the (002) direction, which is consistent with the XRD spectra to be presented in a later paragraph. Some lattice mismatch in the film is noted. No significant diffusion across the film/substrate interface was observed. The diffraction pattern (inset to the HRTEM image of Fig. 1(a)) taken at the interface shows no presence of secondary phase nor precipitation. The SIMS depth profile of the as-grown ZnO:Sb(1%) sample is shown in Figure 1(c), revealing a rather uniform distribution of Zn, O, and Sb through the whole film, and no segregation was observed. The Sb concentrations in the as-grown ZnO:Sb(0.5%), ZnO:Sb(1%), ZnO(2%) and ZnO(3%) samples are respectively 1×10^{20} cm^{-3}, 2×10^{20} cm^{-3}, 4×10^{20} cm^{-3} and 1×10^{21} cm^{-3} as revealed by the SIMS measurements.

Figure 1(b) shows the XRD spectra of the as-grown ZnO:Sb(0.5%), ZnO:Sb(1%), ZnO(2%) and ZnO(3%) samples with the intensity plotted in log scale. The intensities of the (100), (101), (103) and (200) peak observed in Figure 1(b) are negligible as compared to that of (002) peak (~100 times less than that of (002) peak). The dominance of the (002) peak revealed the preferential c-axis orientation wurtzite structure of the samples. The lattice constant derived from the (002) peak positions are 5.19 Å, 5.21 Å, 5.21 Å and 5.36 Å for the samples ZnO:Sb(0.5%), ZnO:Sb(1%), ZnO(2%) and ZnO(3%) respectively. The moderate increase of the lattice constant from 5.19 Å to 5.21 Å with increasing Sb composition from 0.5 % to 2 % could be

due to the occupation of the large Sb^{3+} (0.76Å) ions into Zn^{2+} sites (0.6Å). As the Sb composition further increases from 2 % to 3 %, the lattice constant abruptly increases from 5.21 Å to 5.36 Å. This is associated with the occupation of Sb into the O-site [22,23] and more discussion will be given in the coming paragraphs.

The electron concentrations of the Sb-doped ZnO samples fabricated with different Sb composition and annealed at different temperatures are tabulated in Table I. All the samples exhibited n-type conductivity. For the as-grown Sb-doped ZnO samples, the electron concentration increases from 1×10^{20} cm^{-3} to 3×10^{20} cm^{-3} as Sb composition increases from 0.5 % to 2 %. Further increasing the Sb composition to 3 % leads to abrupt decrease of electron concentration to 4×10^{14} cm^{-3}. The initial increase of electron concentration with Sb composition with low Sb concentration is due to the increase of the Sb_{Zn}-related shallow donor [22,23]. The abrupt drop of electron concentration was due to the formation of Sb_O acceptor at large Sb composition compensating the material [22,23], which was also evidenced by the abrupt increase of lattice constant observed in the current XRD study.

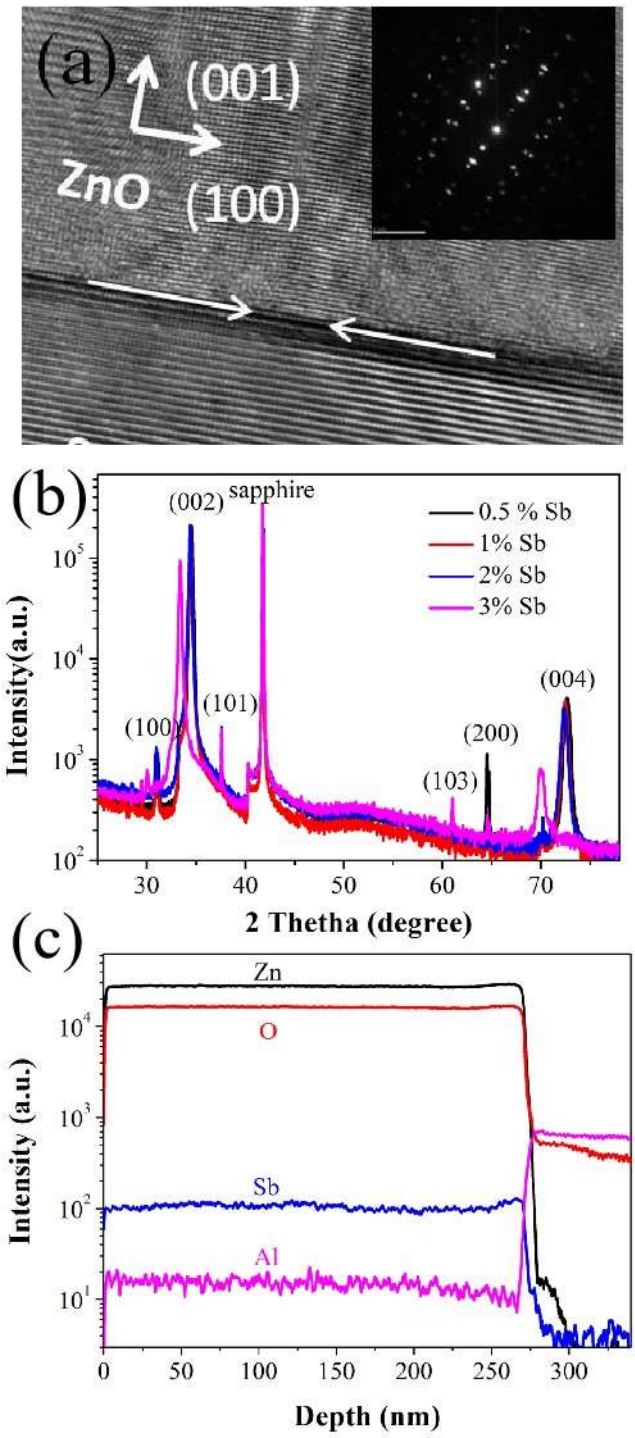

Figure 1 (a) The HRTEM image of the film/substrate interface for the as-grown ZnO:Sb(2%) sample. The insert shows the diffraction pattern taken at the film/substrate interface, showing absence of secondary phase nor significant diffusion; (b) The XRD spectra of the Sb-doped ZnO samples with different Sb compositions; (c) The SIMS depth profiles of Zn, O, Sb and Al for the as-grown ZnO:Sb(1%) sample.

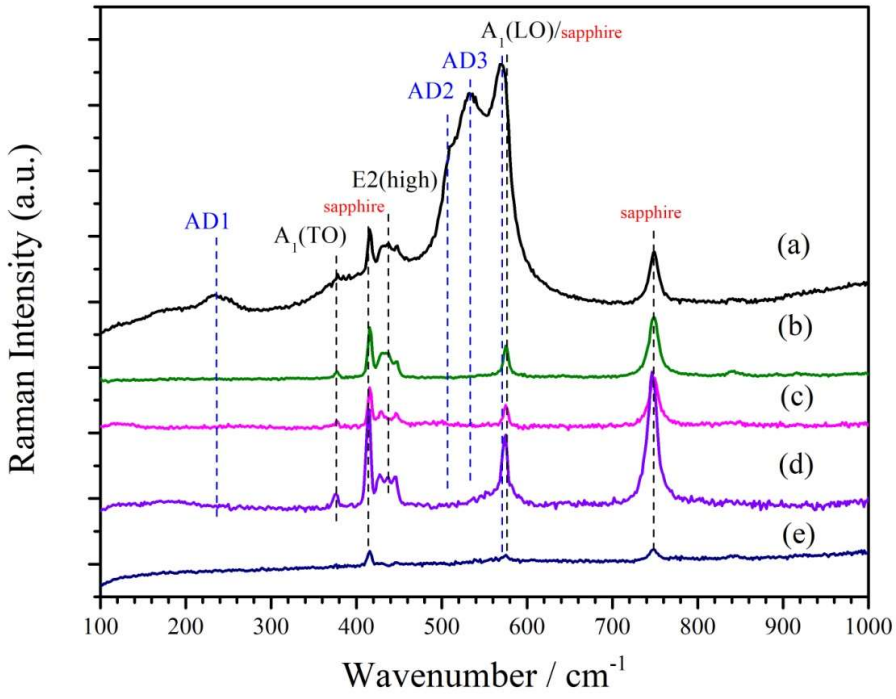

Figure 2 The Raman spectra of the undoped ZnO film and doped ZnO films with different dopant (a) 1% wt Sb doped ZnO; (b) 1% wt Ga doped ZnO; (c) 1% wt Cu doped ZnO; (d) undoped ZnO; and (e) sapphire substrate.

Table I Electron concentration of the as-grown Sb-doped ZnO samples having different Sb compositions, ZnO:Sb(2%) samples annealed at different temperatures and the control as-grown undoped ZnO sample.

Sample		n (cm^{-3})
Undoped ZnO	As grown	1.32×10^{18}
0.5 wt % Sb	As grown	1.08×10^{20}
1.0 wt % Sb	As grown	1.40×10^{20}
2.0 wt % Sb	As grown	3.26×10^{20}
	500 °C annealed	1.85×10^{20}
	600 °C annealed	3.75×10^{18}
	700 °C annealed	5.50×10^{16}
3.0 wt % Sb	As grown	3.70×10^{14}

Table II Raman modes observed in the Sb-doped ZnO samples, undoped ZnO control sample, Ga-doped ZnO sample, Cu doped ZnO sample and the sapphire substrate. These Raman modes are observed in the corresponding Raman spectra shown in Figure 2.

Sample	Vibration modes (cm^{-1})							
ZnO:Sb 1%	235	378	416	437	510	534	570	749
ZnO:Ga 1%		378	416	437			575	749
ZnO:Cu 1%		378	416	437			575	749
Undoped		378	416	437			575	749
substrate			416				575	749

Figure 2 shows the Raman spectra of the sapphire substrate, the undoped ZnO, and ZnO thin films doped with the different dopants Sb, Ga and Cu. The phonon frequencies of the observed Raman peaks are tabulated in Table II. The Raman vibrations 416 cm^{-1}, 575 $cm^{-1}$and 749 cm^{-1} observed in the Raman spectra of the sapphire substrate are undoubtedly associated to c-sapphire. These three peaks were also observed in the four ZnO samples, which would be originated from the substrate. However, it is worthy to have more discussion on the 575 cm^{-1} peak. Raman mode of A_1 (LO) peaking at 575 cm^{-1} has been reported in ZnO. Thus, the 575 cm^{-1} Raman peak observed in the current undoped Cu-doped and Ga-doped ZnO samples could be co-contributed from the ZnO film and the sapphire substrate. For the Sb-doped ZnO, the 575 cm^{-1} peak red-shifted to 570 cm^{-1}. Similar red shift was also reported previously [24,25] and the 570 cm^{-1} Raman mode in Sb-doped ZnO could be related to Sb-doping. The Raman modes 378 cm^{-1} and 437 cm^{-1} observed in all the ZnO samples of the current study have been referred to vibrational modes A_1 (TO) and E_2 (high) respectively [26]. The E_2 (high) mode [27,28] of ZnO was associated

to the vibration of oxygen atoms. The E_2 (low) Raman signal of ZnO reported in other literature [27,28] associated with the vibration of Zn atoms was not detected in the present samples. Other than the A_1 (LO), A_1 (TO) and E_2 (high) modes, three additional modes at 235cm^{-1} (AD1), 510 cm^{-1} (AD2), 534 cm^{-1} (AD3) were observed in the current study only in the Sb doped ZnO samples but not in the other undoped, Cu-doped nor Ga-doped ZnO samples.

As Sb-related secondary phase is not detected in the XRD spectrum nor in the TEM image of the Sb-doped ZnO samples (Figure 1(a) and (b)), it is not likely that the AD1, AD2 and AD3 modes are associated with the Sb-related secondary phase like Sb oxide. Based on the considerations of atomic size and formation energy, Sb occupies the Zn sites (Sb_{Zn}) rather than the O sites [29,30]. The relation between the local vibration modes (LVM) ω and the effective mass μ of the Zn site and Sb_{Zn} is given by [31,32]:

$$\frac{\omega_{LVM}}{\omega_{Zn-O}} = \sqrt{\frac{\mu_{Zn-O}}{\mu_{LVM}}} \qquad (1)$$

The Sb-related LVM frequency can be estimated from the effective mass of the LVM and ZnO, which are given by: $\mu = (M^{-1} + m^{-1})^{-1}$. Taking the value ω_{Zn-O}=437 cm-1 for E_2 (high), $\mu_{Zn-O}/\mu_{LVM} = 0.30$ was obtained by using the relative atomic mass of the relevant elements. The LVM frequency for Sb-Zn pair was calculated to be 240 cm^{-1}, which was close to that of AD1 (235 cm^{-1}). This indicates the relation between AD1 and Sb_{Zn} [27].

The AD2 mode at 510 cm^{-1} has previously been observed in the Raman spectra of N, Fe, Sb and Al doped ZnO thin films, as well as in the Ga-doped ZnO sample grown with N_2O gas [17,33]. The origin of AD2 is still controversial. This mode is usually associated with the native crystal imperfection, defects or impurities. Manjon et al [34] compared the experimental results with the ab initio calculations of the lattice dynamics in wurtzite ZnO. It was proposed that many of the anomalous bands including the 510 $cm^{-1}$are related to the silent Raman modes associated with the breakdown of the translational symmetry of the crystal lattice. Dong et al [35] observed two silent modes at 275 cm^{-1} and 511 cm^{-1} from the H-plasma treated and annealed ZnO sample, which was associated with the H_O defects. As AD2 has been observed in ZnO doped with many different dopants, AD2 is not associated with the Sb dopant, but rather be associated with native defects or H that are commonly found in ZnO samples.

The vibrational mode 534 cm^{-1} (AD3) has also been reported in the Raman study of Bundesmann et al [17], which was specifically associated with the Sb incorporation into ZnO. However, its exact structure of the corresponding Sb-related defect is not known yet.

Figure 3 (a) shows the Raman spectra of the ZnO:Sb(1%) samples annealed at the different temperatures, which clearly shows the decrease of the additional modes intensities with the increasing annealing temperature. The broad band in the range of 460-640 cm^{-1} was fitted with four modes namely the AD2, AD3, 570 cm^{-1} and the 575

cm^{-1} (see insert of Figure 3(a) showing the broad band of the as-grown sample). The 575 cm^{-1} A_1 (LO) mode was contributed from the sapphire and/or ZnO. The AD2, AD3 and 570 cm^{-1} mode were Sb-doping related. The Lorentzian contribution from the 575 cm^{-1} has had its peak position and FWHM fixed during the fitting. The peak positions of the other modes were also fixed in the fitting while the other parameters ran free. The insert in Figure 3 shows the fitted curves of the resultant and the individual relevant components, for which the fitted resultant curve gives good description to the experimental spectrum.

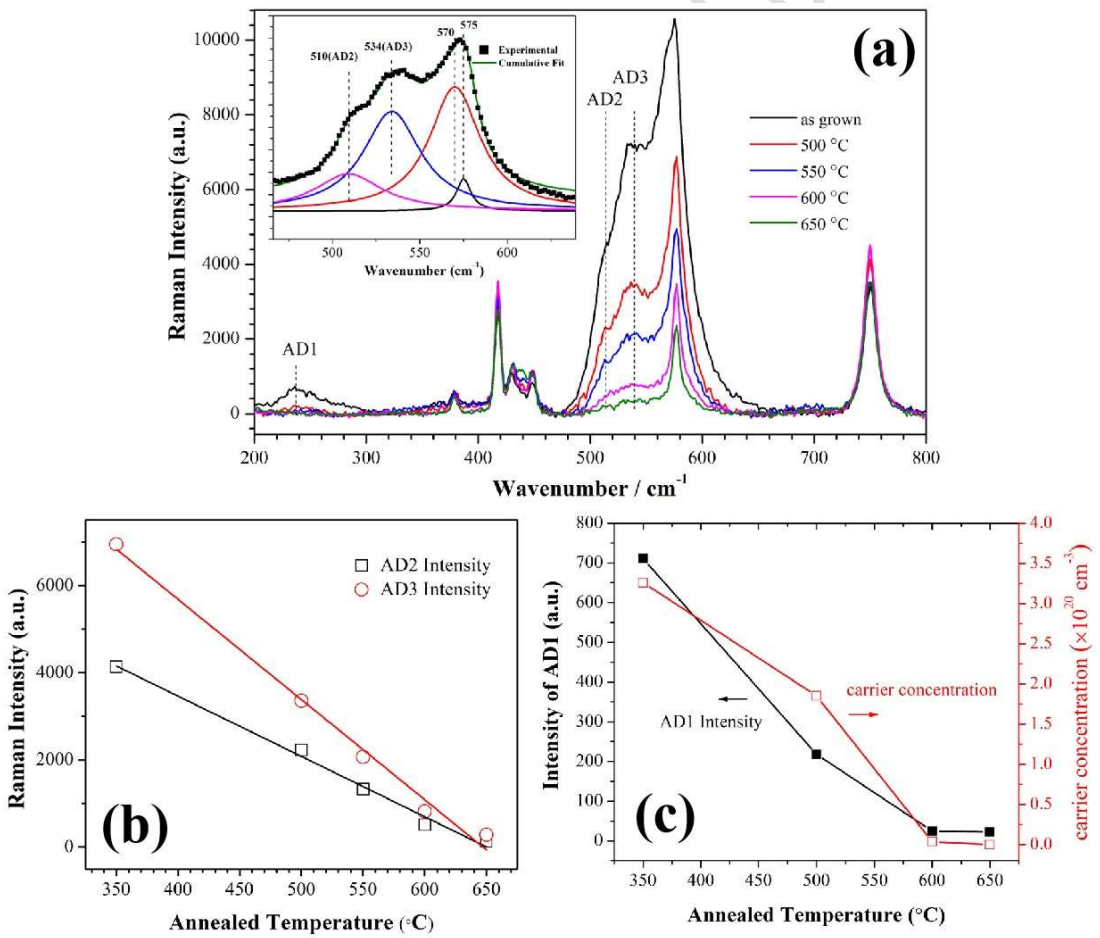

Figure 3 (a) The Raman spectra of the ZnO:Sb(1%) samples annealed at different temperatures. The insert shows the fitting of the broad band from 460-640 $cm^{-1}$by the Lorentzians peaking at 510 cm^{-1} (AD2), 534 cm^{-1} (AD3), 570 cm^{-1} and 575 cm^{-1} (A_1 (LO)). The resultant fitting curve is also included; (b) The intensities of the Raman additional modes AD2 and AD3 against the annealing temperature for the ZnO:Sb(1%) samples; and (c) The intensity of the Raman additional mode AD1 and the electron concentration as a function of the annealing temperature for the ZnO:Sb(1%) samples.

The intensities of AD2 and AD3 as shown in Figure 3 (c) drop gradually with increasing annealing temperature and become nearly zero as the annealing temperature reaches 650 ℃. AD2 has been associated with H_O and crystalline defects in previous literature [35]. First principles calculations and kinetic Monte Carlo simulation studies showed that H_O maintained thermally stable up to 475 ℃ [36], which agreed with the results of nuclear reaction analysis study performed on As-doped ZnO [37]. The drop of the present AD2 intensity could be due to the thermal removal of H_O or the related intrinsic defect. The decrease of the AD3 intensity could be associated to the annealing out of the corresponding Sb-related defect.

Figure 3(d) shows the correlated variations of AD1 intensity and the electron concentration as a function of the annealing temperature. AD1 intensity drops to nearly zero (by a fraction of 96 %) after annealing at 600 ℃, while at the same time the electron concentration abruptly drops from ~3×10^{20} cm^{-3} to ~4×10^{18} cm^{-3}. We have studied the Sb-doped ZnO films fabricated by the similar PLD method as the as the present study using a comprehensive spectroscopic approach including XRD, Hall

measurement, photoluminescence (PL), X-ray photoelectron spectroscopy (XPS) and coincidence Doppler broadening spectroscopy (CDBS) [15]. CDBS is a kind of positron annihilation spectroscopy selectively sensitive for the electronic momentum distribution around the V_{Zn}-related defects and thus can reveal the impurity decoration of the V_{Zn} defect. Comparing with the electronic momentum distribution obtained from a control Sb sample and the as-grown Sb-doped ZnO sample (Sb=2 %), the V_{Zn} in the Sb-doped ZnO sample after 750 ^{o}C annealing was found to be decorated by the Sb impurity. This was correlated with the decrease of electron concentration from the as-grown value of ~10^{20} cm^{-3} to ~10^{17} cm^{-3}, and the introduction of the 3.32 eV emission in the 10 K PL spectrum after the annealing. The 3.32 eV emission was attributed to the free-to-acceptor emission involving an acceptor at E_V+120 meV (E_V is the valence band maximum). First principles calculation showed that Sb_{Zn}-$(V_{Zn})_2$ was a shallow acceptor having low formation energy with the state at E_V+160 meV [14], which was close to acceptor involved in the FA transition. It was thus concluded that the annealing initiated the V_{Zn} diffusion and thus the formation of the Sb_{Zn}-$(V_{Zn})_2$ shallow acceptor, which consequently compensated the electron concentration and introduced of the FA line in the PL spectrum. Similar results of the formation of As_{Zn}-$(V_{Zn})_2$ shallow acceptor and thermal annealing behavior were also reported in the sputtering grown As-doped ZnO film [38,39]. As suggested in the vibrational mode frequency analysis in the previous paragraph, the vibrational mode AD1 is associated with the Sb_{Zn} site. The reduction in electron concentration after annealing at 600 ^{o}C (Figure 3(c)) is attributed to the removal of the Sb_{Zn} shallow

donor with the formation of Sb_{Zn}-$(V_{Zn})_2$ shallow acceptor, which compensates the electron concentration. The correlated drop of the AD1 intensity is associated with the removal of its origin Sb_{Zn} while it converts to Sb_{Zn}-$(V_{Zn})_2$.

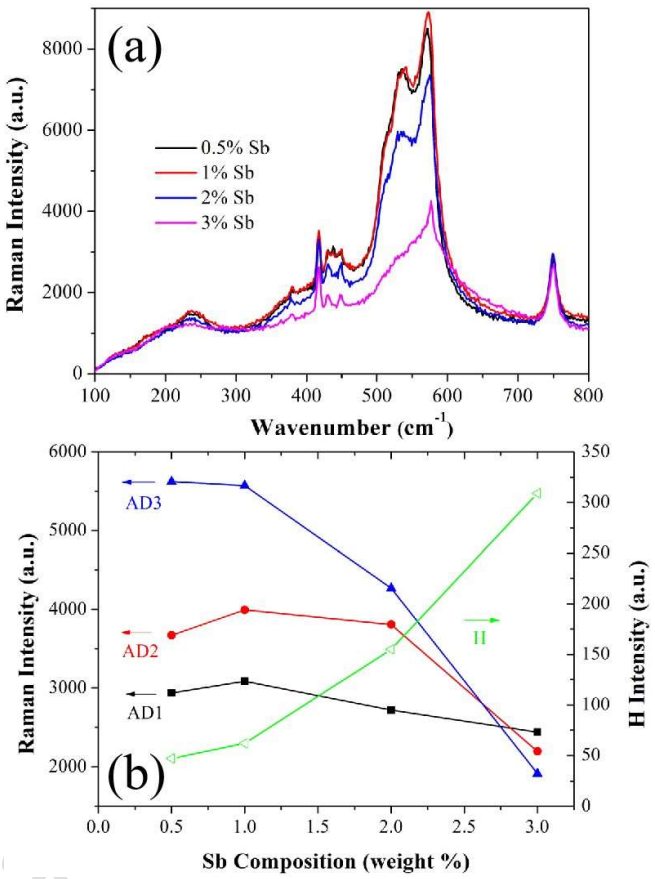

Figure 4 (a) The Raman spectra of the as-grown Sb-doped ZnO samples with different Sb doping compositions; and (b) The intensities of Raman additional modes AD1, AD2 and AD3 as a function of the Sb composition for the as-grown Sb-doped ZnO samples. The hydrogen abundance revealed by SIMS against the Sb composition in the samples are also included.

Figure 4(a) shows the Raman spectra of the Sb-doped ZnO sample doped with different Sb composition. The additional vibrations AD1, AD2, AD3 were observed

in all the Sb doped ZnO films. It is clearly seen that the intensities of AD1, AD2 and AD3 drops with increasing Sb composition, for which their intensities against the Sb composition are shown in Figure 4(b). As AD2 may be associated with H_O, it would be worthy to study the H abundance in the samples having the different Sb compositions. The H abundance of each of the samples were studied by SIMS, and the corresponding relative H abundances were included in Figure 4(b). For Sb increasing from 0.5 % to 2.0 %, the H-intensity moderately increases with the Sb composition by a factor ~2, and then increases abruptly by a factor of ~8 as Sb composition increases to 3 %. The increase of H concentration with the increase of Sb composition could hinder the p-type doping by Sb as H could compensate the free holes. The physics leading to the increase of H with increasing Sb doping is unknown and falls outside the scope of the present study. It is worthy to study this in future. Nevertheless, with the increase of Sb composition, the increase in H abundance does not correlate with the trend of the AD2 intensity. There are two possibilities, namely (i) AD2 is not associated with H; (ii) AD2 is associated with H_O and the AD2 intensity drop is related to the microstructure change of the hydrogen (like the occupying site or the defect complex involved) in the sample.

In the same set of samples, the electron concentration drops from ~10^{20} cm^{-3} to <10^{16} cm^{-3} as the Sb concentration is larger than ~8×10^{20} cm^{-3}, correlated with the increase lattice constant from 5.21 Å to 5.36 Å (see XRD results in the previous paragraph and reference[15]). The lattice constant of undoped ZnO film fabricated

by PLD with similar conditions is 5.20 Å. Liu et al [16] observed the same abrupt change of electron concentration and increase of lattice constant as the Sb concentration is larger than the threshold concentration of ~4×10^{20} cm^{-3}. The ionic radii of Sb^{3+} and Zn^{2+} are relatively close in size (0.62 Å and 0.74 Å respectively), and thus the substitution of Sb into the Zn would not significantly deteriorate the lattice structure. However, the ionic radii of Sb^{3-} (2.44 Å) mismatches that of O^{2-} (1.38 Å), implying the substitution of Sb^{3-} into the O^{2-} site would lead to increase in the observed lattice constant. The large lattice constant observed in the samples with high Sb composition was associated with the formation of a Sb-related defect or defect complex having the Sb occupying the O-site [15,16]. Sb_O (and defect complex) was an acceptor that compensate the electron concentration, and this explained the drop in electron concentration [15,16]. The drop of AD1 (which is associated to Sb_{Zn} in the previous paragraph) with increasing Sb composition may be due to the formation of the Sb_O related defect. A similar drop in AD2 intensity is expected if AD2 is also a Sb_{Zn}-related defect. If AD2 is related to H_O, the simultaneous drops of AD1 (related Sb_{Zn}) and AD2 (related to H_O) intensities with increasing Sb composition may be due to the formation of a defect complex involving Sb_O and H, which would decrease the concentrations of isoloated Sb_{Zn} and H_O. A similar acceptor-H complex has been reported by Li et al [40], in which N_O-H defect complex (H at interstitial site) had relatively low formation energy and compensated the N acceptor in N-doped ZnO. These postulations require further investigation.

CONCLUSION

Compared with the Raman spectra of the undoped ZnO, Ga-doped and Cu-doped ZnO samples grown by PLD, three additional modes at 235cm^{-1} (AD1), 511 cm^{-1} (AD2), 534 cm^{-1} (AD3), are observed in the Sb-doped ZnO thin films. The additional modes intensities varied with the Sb concentration, as well as the electron concentration. The ADl mode at 235 cm^{-1} is consistent with the calculated vibration frequency of Sb_{Zn}. It has been reported that Sb_{Zn} is one of the shallow donors in Sb doped ZnO material with activation energy of 5 meV bellow conduction band. The observed AD1 mode could be used for the implication of the presence of Sb_{Zn} shallow donor. The AD2 mode at 511 cm^{-1}, which is also observed in undoped ZnO and ZnO doped with other dopants, has been attributed in previous literatures to the $2B_1$(low) second-order mode related to the breakdown of the translational crystal symmetry with the presence H_O impurities. However in the current study, simple correlation between the AD2 intensity and H concentration was not observed. The AD3 is associated with the Sb-related defect, although the atomic micro-structure is not yet exactly known. The correlation between the electron concentration and the Raman scattering intensities indicates that these additional modes are donor-defect activated and can reveal the electrical property of the Sb-doped ZnO films.

ACKNOWLEDGEMENT

This work was financially supported by the Natural Science Foundation of Guangdong Province – General Program (2019A1515012164).

Reference

[1] Ü. Özgür, Y. I. Alivov, C. Liu, A. Teke, M. Reshchikov, S. Doğan, V. Avrutin, S.-J. Cho, and H. Morkoc, Journal of applied physics **98**, 11 (2005).
[2] X. Yu, T. J. Marks, and A. Facchetti, Nature materials **15**, 383 (2016).
[3] R. A. Zargar, M. Arora, and R. A. Bhat, Applied Physics A **124**, 36 (2018).
[4] D. M. Hofmann, A. Hofstaetter, F. Leiter, H. Zhou, F. Henecker, B. K. Meyer, S. B. Orlinskii, J. Schmidt, and P. G. Baranov, Physical Review Letters **88**, 045504 (2002).
[5] D. Thomas and J. Lander, The Journal of Chemical Physics **25**, 1136 (1956).
[6] L. Liu, Z. Mei, A. Tang, A. Azarov, A. Kuznetsov, Q.-K. Xue, and X. Du, Physical Review B **93**, 235305 (2016).
[7] K. Vanheusden, C. Seager, W. t. Warren, D. Tallant, and J. Voigt, Applied physics letters **68**, 403 (1996).
[8] X. Wu, G. Siu, C. Fu, and H. Ong, Applied Physics Letters **78**, 2285 (2001).
[9] Y. Frodason, K. Johansen, T. Bjørheim, B. Svensson, and A. Alkauskas, Physical Review B **95**, 094105 (2017).
[10] Z. Wang *et al.*, Scientific reports **9**, 3534 (2019).
[11] Z. Y. F. X. Xiu, L. J. Mandalapu, D. T. Zhao, J. L. Liu, Applied Physics Letters **87**, 252102 (2005).
[12] C. Y. Z. J. C. Fan, S. Fung, Y. C. Zhong, K. S. Wong, Z. Xie, G. Brauer, W. Anwand, W. Skorupa, C. K. To, B. Yang, C. D. Beling, and C. C. Ling, Journal of Applied Physics **106**, 073709 (2009).
[13] C. K. To, B. Yang, S. C. Su, C. C. Ling, C. D. Beling, and S. Fung, Journal of Applied Physics **110** (2011).
[14] S. Limpijumnong, S. Zhang, S.-H. Wei, and C. Park, Physical review letters **92**, 155504 (2004).
[15] C. Luo *et al.*, Journal of Applied Physics **123**, 161525 (2018).
[16]H. Liu, N. Izyumskaya, V. Avrutin, Ü. Özgür, A. Yankovich, A. Kvit, P. Voyles, and H. Morkoç, Journal of Applied Physics **112**, 033706 (2012).
[17] C. Bundesmann, N. Ashkenov, M. Schubert, D. Spemann, T. Butz, E. M. Kaidashev, M. Lorenz, and M. Grundmann, Applied Physics Letters **83**, 1974 (2003).
[18] R. Kirste, Y. Aksu, M. R. Wagner, S. Khachadorian, S. Jana, M. Driess, C. Thomsen, and A. Hoffmann, ChemPhysChem **12**, 1189 (2011).
[19] J. Zuo, C. Xu, L. Zhang, B. Xu, and R. Wu, Journal of Raman Spectroscopy **32**, 979 (2001).
[20] K. M. Paradowska, E. Przeździecka, E. Płaczek-Popko, E. Zielony, M. Stachowicz, and A. Kozanecki, Journal of Alloys and Compounds **774**, 1160 (2019).
[21] E. Przezdziecka, K. M. Paradowska, W. Lisowski, A. Wierzbicka, R. Jakiela, E. Zielony, Z. Gumienny, E. Placzek-Popko, and A. Kozanecki, Journal of Alloys and Compounds **797**, 1163 (2019).
[22] C. Luo *et al.*, Journal of Applied Physics **123** (2018).
[23] H. Y. Liu, N. Izyumskaya, V. Avrutin, Ü. Özgür, A. B. Yankovich, A. V. Kvit, P. M. Voyles, and H. Morkoç, Journal of Applied Physics **112**, 033706 (2012).

[24] K. Paradowska, E. Przeździecka, E. Płaczek-Popko, E. Zielony, M. Stachowicz, and A. Kozanecki, Journal of Alloys and Compounds **774**, 1160 (2019).
[25] E. Przezdziecka, K. Paradowska, W. Lisowski, A. Wierzbicka, R. Jakiela, E. Zielony, Z. Gumienny, E. Placzek-Popko, and A. Kozanecki, Journal of Alloys and Compounds **797**, 1163 (2019).
[26] F. Decremps, J. Pellicer-Porres, A. M. Saitta, J.-C. Chervin, and A. Polian, Physical Review B **65**, 092101 (2002).
[27] N. K. Singh, S. Shrivastava, S. Rath, and S. Annapoorni, Applied Surface Science **257**, 1544 (2010).
[28] Y.-I. Kim, S. Cadars, R. Shayib, T. Proffen, C. S. Feigerle, B. F. Chmelka, and R. Seshadri, Physical Review B **78**, 195205 (2008).
[29] U. Wahl, J. Correia, T. Mendonça, and S. Decoster, Applied Physics Letters **94**, 261901 (2009).
[30] U. Wahl, E. Rita, J. Correia, A. Marques, E. Alves, J. Soares, and I. collaboration, Physical review letters **95**, 215503 (2005).
[31] K. Samanta, P. Bhattacharya, and R. S. Katiyar, Journal of Applied Physics **108**, 113501 (2010).
[32] A. Kaschner, H. Siegle, G. Kaczmarczyk, M. Straßburg, A. Hoffmann, C. Thomsen, U. Birkle, S. Einfeldt, and D. Hommel, Applied Physics Letters **74**, 3281 (1999).
[33] A. Kaschner *et al.*, Applied Physics Letters **80**, 1909 (2002).
[34] F. J. Manjón, B. Marí, J. Serrano, and A. H. Romero, Journal of Applied Physics **97**, 053516 (2005).
[35] J. Dong *et al.*, ACS applied materials & interfaces **2**, 1780 (2010).
[36] J. Bang and K.-J. Chang, Applied physics letters **92**, 132109 (2008).
[37] J. C. Fan *et al.*, Semiconductor Science and Technology **25**, 085009 (2010).
[38] J. C. Fan *et al.*, Journal of Applied Physics **106**, 073709 (2009).
[39] C. K. To, B. Yang, S. C. Su, C. C. Ling, C. D. Beling, and S. Fung, Journal of Applied Physics **110**, 113521 (2011).
[40] X. Li, B. Keyes, S. Asher, S. B. Zhang, S.-H. Wei, T. J. Coutts, S. Limpijumnong, and C. G. V. d. Walle, Applied Physics Letters **86**, 122107 (2005).